Dynamics of Polystyrene Melts through Hierarchical Multiscale Simulations

Vagelis A. Harmandaris* and Kurt Kremer

Max-Planck-Institut für Polymerforschung, Ackermannweg 10, D-55128 Mainz, Germany

Received August 15, 2008; Revised Manuscript Received November 27, 2008

ABSTRACT: A quantitative understanding and prediction of the dynamics of entangled polymer melts is a long-standing problem. In this work we present results about the dynamical and rheological properties of atactic polystyrene melts, obtained from a hierarchical approach that combines atomistic and coarse-grained dynamic simulations of unentangled and entangled systems. By comparing short chain atomistic and coarse-grained simulations, the time mapping constant is determined. Self-diffusion coefficients, after correcting for the chain end free volume effect, show a transition from Rouse to reptation-like behavior. In addition, the entanglement molecular weight is calculated through a primitive path analysis. All properties are compared to experimental data.

1. Introduction

Understanding the dynamics and the rheology of polymers is a long-standing problem, which has been extensively studied through various experimental and theoretical approaches.[1−3] Complementary to experiments and to analytical theory, molecular simulation techniques are a very useful tool for studying the dynamical properties of polymeric materials.[4−8] On the microscopic level, atomistic molecular dynamics simulations have been used for the prediction of chain diffusion of polymers with simple chemical structure, like polyethylene or polybutadiene, and with low molecular weight.[8−10] However, because of the broad range of length and time scales characterizing macromolecules, application of these techniques to systems with high molecular weight or to polymers with more complicated structure is not possible in most cases.[5,6,8−11] For this reason and in order to increase the length and time scales accessible by simulations coarse-grained (CG) models have proven to be very efficient.[6]

Coarse-grained molecular models are obtained by lumping groups of chemically connected atoms into "superatoms" and deriving the effective, coarse-grained interaction potentials from the microscopic details of the atomistic models. This is to be distinguished from ad hoc coarse-grained models, like simple bead spring or lattice models, which are very useful to study generic scaling properties but lack a link to specific systems.[4,5,7] The development of coarse-grained particle-based models for specific polymers is a very active research field, and various models and methods have been proposed in the literature.[11−30] These CG models differ in the way the effective CG potentials are derived and also in the degree of coarse-graining. For structure-based CG models, the direct link to the chemistry is achieved through structurally defined bonded and nonbonded effective CG potentials derived from the atomistic model. By doing that, the structural properties of the polymeric systems, on both the monomer and the chain dimension level, can be described quite well. However, such CG MD simulations cannot be used directly for a *quantitative* study of the dynamics of polymer systems because the time in the CG description does not correspond to the real physical time of the underlying chemistry. Because of the lost degrees of freedom in the CG description, the effective CG potentials are softer compared to the atomistic ones. This results in a reduced effective friction between the beads. A way to overcome this limitation is by performing a "scaling" of the CG time using data taken either from experiments or from atomistic simulations. Finally, more coarser particle models, where the chemistry takes place through some phenomenological parameters, have also been developed.[31−36] The parameters characterizing such models are usually obtained by proper fitting of a dynamical quantity to experimental data.

Polystyrene (PS) is a common commercial polymer and one of the experimentally most widely studied among all amorphous polymers.[1,37−44] In addition, molecular modeling techniques have also been applied for the study of polystyrene. Modeling at the atomistic level, using either molecular dynamics (MD)[45−50] or Monte Carlo[51] simulations, has been used to study mainly structural and some short time local dynamical aspects of bulk atactic PS. During the past few years, a few different coarse-grained models of PS have also been presented in the literature.[17,18,20−22,52] These models vary in the degree of coarse-graining as well as in the procedure for obtaining the effective interactions between the CG beads (superatoms), i.e., the CG force field.

Recently, we have developed a CG model for PS in which each PS monomer is represented by two superatoms (2:1 CG model). The CG model has been developed by employing a structure-based CG methodology that combines atomistic and CG simulations.[52] This model can describe PS sequences with varying tacticities and has been tested and validated for a number of structural and dynamical properties of atactic polystyrene[17,52] as well as of polymer/penetrant binary mixtures.[53] Furthermore, the CG PS model was used to study the mechanical properties of PS glasses.[54,55] In the present work, we extend this approach to study dynamical and rheological properties of various monodisperse PS melts of molecular weight below and well above the entanglement threshold, M_e. The results are obtained mainly from the CG MD simulations. However, the hierarchical modeling of atomistic and CG MD simulations in some reference systems allows us to define correctly the time scale in the CG runs and to quantitatively predict dynamic properties of the PS melts through the CG simulations without any adjustable parameter.[56] Following this methodology, the results from the CG simulations can be directly compared to experimental data.

The paper is organized as follows. First, a brief overview of the atomistic and the coarse-graining simulations performed in this work is given in the next section. In section 3 basic structural properties are presented. The time mapping aspect is discussed

* To whom correspondence should be addressed.

10.1021/ma8018624 CCC: $40.75
Published on Web 01/13/2009

Table 1. Atomistic Simulated PS Systems Studied in the Present Work (T = 463 K)

model	M (kDa)	no. of chains	ρ (g/cm^3)	simul time (ns)
UA	1	45	0.925	50
UA	2	32	0.940	100
UA	3	27	0.950	300
UA	5	32	0.955	300
UA	10	32	0.965	300
AA	1	56	0.925, 0.940, 0.950, 0.955, 0.965, 0.97	300

in section 4. Section 5 presents results on the segmental, as well as the chain center of mass, dynamics of PS melts. A detailed entanglement analysis is described in section 6. Finally, our findings and conclusions are summarized in section 7.

2. Simulation Methodology

2.1. Atomistic Simulations of Polystyrene. The hierarchical approach presented here involves atomistic, united-atom (UA) and CG dynamic simulations of atactic PS melts. The sequence of atomistic and UA simulations is needed in order to parametrize the time scale in the CG description. UA MD simulations have been performed using the TraPPE UA model,[57] based on which the CG model was parametrized. In this model each PS monomer is described with eight united atom groups. Five different types of united atoms (CH_3, CH_2, CH, C_{aro}, and CH_{aro}) are defined in a PS chain, whose nonbonded interactions are described by pairwise-additive Lennard-Jones potentials. All bond lengths are kept rigid, whereas a harmonic potential is used to describe bond angle bending. Standard torsional potentials are used to describe rotations along bonds in the aliphatic backbone. These dihedral potentials count also for the 1−4 nonbonded interaction. Finally, improper dihedral potentials are used to keep the phenyl ring planar as well as to maintain the tetrahedral configuration around the sp^3-hybridized carbon connecting the phenyl ring. Using this UA model, we performed atomistic MD simulations for various atactic PS melts with molecular weight, M, ranging from 1 to 10 kDa (see Table 1, 1 kDa = 1000 g/mol).[17]

UA models have the advantage to be more efficient than all-atom ones for long MD simulations since hydrogens are not treated explicitly. In addition, they are usually considered to be "atomistic" in the sense that the time scale does not deviate in a detectable way from all atom simulations because the "coarse-graining" of the UA models is of the order of hydrogen−carbon bond, i.e., only about 1 Å. However, this assumption, which in many cases (for example, UA models for PE, PB, and PI)[4,8−10] works reasonably well, fails to work for the UA-TraPPE PS model; i.e., it predicts for PS a much faster dynamics.[52,56] This is most probably mainly due to too low dihedral barriers along the aliphatic backbone in the UA-TraPPE model. Missing electrostatic interactions and the lumping of hydrogens are expected to be less influential. This however does not affect the overall conformations and the melt structure.[53,52]

Since our goal is to compare *quantitatively* the CG polymer dynamics with experimental data, we decided to parametrize and control the properties of the UA simulations using data by detailed all-atom simulations. Thus, we have also simulated some systems (see Table 1) with a detailed all-atom (AA) PS model, where hydrogens and carbons are treated explicitly.[58] This AA model has partial charges on the carbon and hydrogen atoms of the phenyl groups, which reproduce the electric quadrupole moment of the benzene molecule. Parameters of the barriers for the rotation of polystyrene backbone dihedral angles were calculated from ab initio calculations on polystyrene fragments. For more details of the model see ref 58.

The molecular dynamics package GROMACS[59] was used to perform the atomistic MD simulations. The different PS amorphous systems that have been simulated are presented in

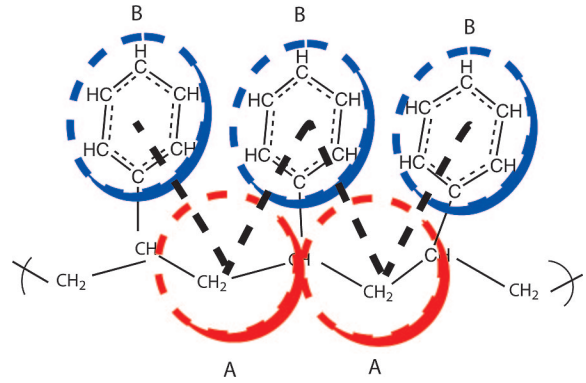

Figure 1. Coarse-graining mapping scheme of PS: one monomer is mapped to two different CG beads (σ_A = 4.1 Å, m_A = 27 amu and σ_B = 5.2 Å, m_B = 77 amu). Dashed lines show CG bonds between CG beads A and B.

Table 1. Initial well-equilibrated atomistic configurations are obtained by back-mapping of the CG melts.[17] UA and AA MD simulations have been conducted under constant temperature and volume (*NVT*) conditions using the Berendsen thermostat (coupling time 0.1 ps).[60] The densities of the simulated melts were chosen to be equal to experimental data,[61] the only direct experimental input for the present study. Note that the pressure in the atomistic simulations is slightly negative since the density predicted by both the UA and the AA force fields is about 3−4% larger than the experimental ones. A negative pressure, induced by the constant volume constraint, of course in principle is unphysical and would lead to inhomogeneities in the system. Here however this is not the case because the fluctuations of instantaneous pressure are about 5−10 times larger than the average (negative) pressure. For much larger systems this can be a problem. Thus, we choose to perform all the simulations at the experimental densities, since later we directly compare with available experimental data. Nonbonded interactions were cut off beyond 1.2 nm. Tail corrections for the energy and pressure were applied.[62] The integration time step was 2 fs for the UA simulations and 1 fs for the AA ones. Finally, the overall atomistic simulation time of the production runs ranged from 50 to 300 ns depending on the molecular weights of the systems studied.

2.2. Coarse-Grained Simulations of Polystyrene. The CG MD simulations have been performed using a CG model for PS in which one PS monomer is mapped onto two effective coarse grained beads.[52] In this model a CG bead "A" includes information from three consequent CH_x groups along the backbone (see Figure 1). In more detail CG bead "A" corresponds to the CH_2 of a PS monomer plus the half-mass of each of the two neighboring CH groups along the chain backbone, whereas CG bead "B" is just the phenyl ring. This model has the advantage of capturing the tacticity without introducing side groups. It was chosen because of mainly two advantages, namely, not losing too many structural details in comparison to the all-atom system, while still being very efficient compared to atomistic simulations. At the same time, due to the rather fine nature of this CG mapping scheme, it is relatively easy to develop a rigorous procedure for reinserting all the atomistic details into the CG configurations.[17] Such a procedure has been also proven quite successful for the case of polycarbonate.[13,63] Furthermore, chain tacticity is captured in our coarse-graining model through the bending and dihedral potentials. More details about the CG model and the procedure to obtain the CG force field can be found elsewhere.[17,52,53]

All systems modeled by CG simulations in this study are presented in Table 2. In all cases, the chains are generated by a MC algorithm[17,64] with all the bond lengths as well as bending

Table 2. Coarse-Grained PS Systems Studied in the Present Work ($T = 463$ K)

M (kDa)	no. of beads per chain	no. of chains	$\langle R^2 \rangle$ (Å^2)	$\langle R_G^2 \rangle$ (Å^2)
1	20	480	180.0 ± 20.0	35.0 ± 5.0
2	40	240	450.0 ± 30.0	75.0 ± 5.0
3	60	160	740.0 ± 50.0	118.0 ± 8.0
5	96	100	1290.0 ± 100.0	205.0 ± 10.0
8	153	60	2250.0 ± 150.0	360.0 ± 20.0
10	192	50	2900.0 ± 300.0	460.0 ± 30.0
12.5	240	50	3800.0 ± 300.0	590.0 ± 50.0
15	288	50	4600.0 ± 320.0	720.0 ± 70.0
20	384	50	6500.0 ± 400.0	1050.0 ± 100.0
25	480	50	8200.0 ± 500.0	1300.0 ± 120.0
30	576	50	10600.0 ± 600.0	1750.0 ± 140.0
40	768	50	14300.0 ± 600.0	2400.0 ± 160.0
50	960	50	17800.0 ± 700.0	2950.0 ± 200.0

and dihedral angles of the CG chains obtained from the CG bonded effective potentials. The coarse-grained chains are randomly placed in the cubic simulation box, thereby introducing significant local density fluctuations across the box. For systems with M from 20 kDa, we create initial random walks with end-to-end distance close to the average one.[17,64,66] This choice improves the starting configurations and is needed because of the small size of the simulated system (we have only 50 chains in the simulation box). To decrease the density fluctuations, we perform a zero temperature Monte Carlo simulation.[64] Also, MD simulations have been performed in dimensionless LJ units using m_A to scale all masses, $\sigma_{AV} = (\sigma_A + \sigma_B)/2$ to scale all lengths and $\epsilon = kT$ to scale all energies. The initially generated chains are still strongly violating the excluded volume constraints. To eliminate this effect, the intermolecular interaction potential is introduced slowly. In order to control the temperature in the system, we use a Langevin thermostat with friction coefficient $\Gamma = 1.0\tau^{-1}$. Once the bead bead overlap disappears, we introduce full nonbonded interaction potentials to perform the MD simulations. Internal distances along the backbone have been monitored throughout the whole equilibration procedure.

All coarse-grained MD simulations are performed using the ESPResSO package.[65] The size of the box is fixed such that the density of the PS melt is equal to that of the experimentall density. Periodic boundary conditions are used. The time step used in the MD simulations was $\Delta t = 0.01\tau$, where τ is defined as $\tau = (m_A\sigma_{AV}^2/\epsilon)^{1/2}$. We perform MD simulations for times $1 \times 10^4\tau - 3 \times 10^6\tau$ depending upon the system size. Note that even though τ has the unit of time, it is the physical time of the coarse-grained model (for our model $1\tau \simeq 1.71$ ps), rather than that of the underlying polymer with its specific chemical structure and has to be scaled accordingly. Finally, we should also state here that in order to use a larger time step the masses of the two different beads were chosen identical; i.e., we assume that the mass of a monomer is uniformly distributed among the two beads. This assumption has been found to have an effect only on the absolute values of the time mapping and has been studied in more detail elsewhere.[52]

3. Structural Properties

We first study the structural and conformational properties of the atactic PS melts studied through CG MD simulations. The results are compared against experimental data and used to ensure that the CG PS melts are well characterized and equilibrated and that their static properties compare well to atactic PS melts at $T = 463$ K.

3.1. Chain Dimensions. Figure 2 and Table 2 present the mean-squared end-to-end distance, $\langle R^2 \rangle$, and the mean-squared radius of gyration, $\langle R_G^2 \rangle$, as a function of chain length N. Note that $N = 2N_{mon}$ with N_{mon} being the number of monomers (repeat

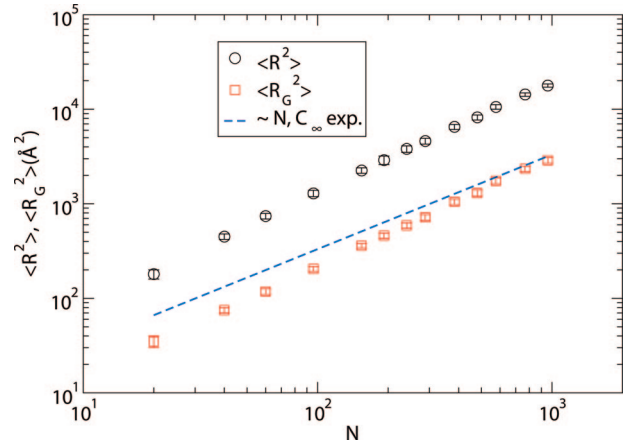

Figure 2. Mean-square end-to-end distance, $\langle R^2 \rangle$, and radius of gyration, $\langle R_G^2 \rangle$, as a function of chain length N ($T = 463$ K). Line shows the $\langle R_G^2 \rangle$ values predicted from the random coil hypothesis using the experimental value of C_∞.

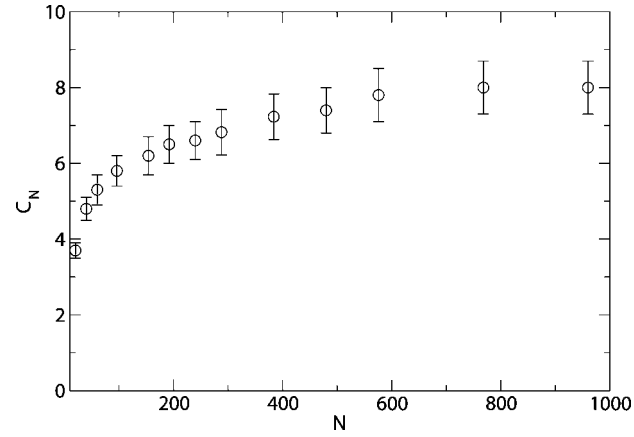

Figure 3. Characteristic ratio as a function of chain length N ($T = 463$ K).

units). It can be seen that as length of the PS in the melt is increasing, $\langle R_G^2 \rangle$ is approaching the value predicted by the random coil hypothesis (linear N dependence, dash line) using the experimental value of C_∞.[66] The ratio $\langle R^2 \rangle / \langle R_G^2 \rangle$ is close to 6 for the high molecular weight systems (above 20 kDa), as expected for random walk statistics, which the polymer chains in the melt should follow. Note also that results obtained for the short PS chains (up to 30 monomers) from the long atomistic MD simulations (up to 0.3 μs) are, as expected, in excellent agreement with that from the coarse-grained simulations.[52]

The characteristic ratio C_N can be calculated from the mean-squared end-to-end distance as a function of chain length N through $C_N = \langle R^2 \rangle / ((N-1)l^2)$, where l is the atomistic backbone bond length ($l = 1.53$ Å) and $(N-1)$ is the number of backbone bonds. Results about C_N are shown in Figure 3 for the systems studied here. As expected from theory, as the length of the PS chain is increasing, C_N approaches a plateau value of ~8.0 for all chain lengths larger than 250 monomer units that were examined here. This value is close to the expected experimental value of high molecular weight characteristic ratio, C_∞, which is about 8.5 at $T = 463$ K (PS C_∞ is equal to 9.85 at 300 K, corrected for the temperature difference with $d \ln C_\infty / dT = -0.9 \times 10^{-3}$).[66] A more detailed study of the dependence of chain dimensions and C_N on the underlying atomistic model, by comparing our data with an all-atom based CG model, is in progress.[67] Furthermore, our CG PS melts have been checked and analyzed on the level of all internal distances and show full equilibration of the chains at all length scales.[52]

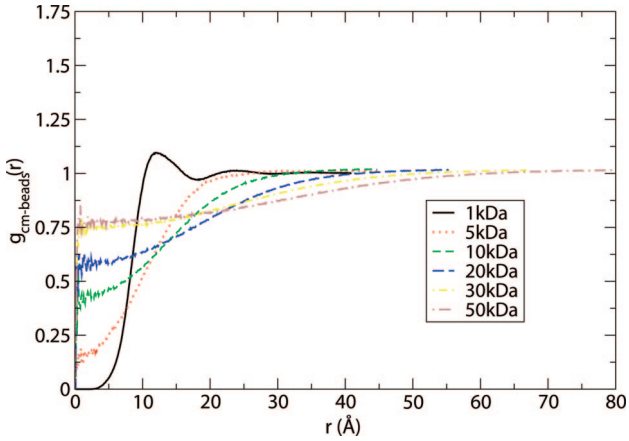

Figure 4. Intermolecular radial distribution function between center-of-mass and individual beads for various PS melts.

The Kuhn length, l_K, can be also calculated, if we consider that it is related to the end-to-end distance as $\langle R^2 \rangle = Ll_K$ with L being the contour length of the chain. Then from the definition of the characteristic ratio and using as contour length the maximum backbone length (all-trans conformation of backbone), i.e., $L = N_K l_K$, we derive

$$l_K = \frac{C_\infty l}{\sin(\theta/2)} \tag{1}$$

with θ being the atomstic backbone bond angle ($\theta = 114°$). Using the plateau value of C_N, the above relation gives a value of $l_K \approx 15.0$ Å.

3.2. Correlation Hole. Direct information about structural features of the polymer systems can be obtained by inspecting the radial distribution functions. Radial distribution functions for correlations between the CG beads, i.e., A−A, B−A, and A−B, have been calculated and found in very good agreement with data obtained from the long atomistic simulations of short PS melts and experimental data.[17,52] Besides the internal structure, of importance is also the overall chain packing, which is directly related with the correlation hole of the polymer chains. For a given chain this can be studied by calculating the intermolecular radial distribution functions of chain beads as a function of distance from the center-of-mass of the test chain, $g_{cm-beads}(r)$. Figure 4 presents $g_{cm-beads}(r)$ for various molecular lengths. The fluctuations at very short distances are due to the small sampling volume. It is obvious that the correlation hole extends over a distance of the order of the average radius of gyration of the chains. Furthermore, the correlation hole is deeper for the shorter chains. Especially for the 1 kDa melt, which consists of only 10 repeat units, the curve shows also a maximum, a typical behavior for short oligomer liquids and not of polymer melts. On the other hand, as the length increases, the correlation hole becomes less deep. This is not surprising if we consider that the volume of a chain is shared with $O(N^{1/2})$ other chains; thus, the degree of interpenetration of the chains increases with chain length. Indeed, for such distances the chain is moving in a soft cage, produced by the environment. This is directly related with the well-known subdiffusive behavior of the chain center-of-mass motion (see below), which for polymer melts results in a characteristic $t^{0.8}$ power law for the mean-square displacement of the center-of-mass on short length and time scales.[9,12,68] Recently, Wittmer et al. relate deviations of the form factor from Debye's formula with a repulsion of segmental correlation holes due to incompressibility and chain connectivity of polymer melts.[69]

4. Time Mapping

The main advantage of CG simulations is that the length and time scales accessible by simulations can be greatly increased. However, as was discussed in the Introduction, the direct use of the "raw" CG data for the *quantitative* predictions of polymer dynamics is not straightforward due to the use of (softer) effective CG potentials. For systems characterized by a scalar friction, such as the homopolymer melts studied here, this can de described as follows:[56] the softer effective CG potentials result in a reduced effective friction coefficient between the beads in the CG description, ζ^{CG}, compared to the friction coefficient in the all-atom detailed atomistic description, ζ^{AA} (i.e., softening of the energy landscape). As a consequence of the softening of the energy landscape at the mesoscopic (CG) description, the time in the dynamic CG simulations does not correspond to the real time of the underlying polymeric system and has to be properly scaled. The scaling parameter, S, is in principle length and time scale dependent and corresponds asymptotically to the ratio between the friction coefficient in the atomistic description and the one in the CG description, i.e., $S = \zeta^{AA}/\zeta^{CG}$ in the sense of the Rouse model. Here we show that "asymptotic" is reached at atomistic scales. Because the local energy landscape is quite complex, it is not possible to give a well-founded analytical prediction of this time scaling parameter S. At the same time, the dependence of this parameter on the system studied and of the state point conditions is of particular importance for the quantitative prediction of polymer dynamics through CG simulations and the transferability of the CG models. This aspect has already been discussed in the literature (see for example refs 13, 17, 53, 52, 24, 63, 70−72, and 56) in the context of "mapping" (scaling) the simulation time at the mesoscopic level to data taken either from experiments or from atomistic simulations.

In order to map the time accurately between the atomistic and the CG length scale, and to calculate the parameter S, one of the following two methods can be used: the first is to equate a scalar dynamical quantity like the diffusion coefficient or the viscosity. The results of the CG model could thus be matched to the value from long atomistic MD runs or experiments. By doing this, only the asymptotic long time regime is being compared. In the case that we do have data from atomistic MD simulations, an alternative way to map the time is to match the mean-square displacement (MSD) of the monomers, the latter providing direct insight into the length scale the particular CG simulations can be used for. The time scaling factor determines the real unit to which the CG time corresponds. Because of the universal nature of the polymer motion on scales above a few beads (Rouse regime), this is more appropriate for our study. Here we follow the last method by using the data of the atomistic and UA simulations of short PS oligomers, with molecular weight up to 10 kDa.

Recently, we followed a three-stage approach in order to study the dependence of the time mapping on the chain length and the density:[56] first UA and CG simulations are performed for molecular weights between 1 and 10 kDa at the experimental densities. This gives the time scaling factor $S_{UA-CG}(M)$. Furthermore, as mentioned before, the TraPPE PS model exhibits a much faster dynamics than the all-atom model. Thus, again we have to follow the same procedure as above, however now for the two models exhibiting atomistic detail. The close match between atomistic and UA simulations at very short distances (data perfectly match from a distance above only about 3 Å)[56] allows us to determine $S_{AA-UA}(M)$ from rather short simulations. With $S_{AA-CG}(M) \equiv \zeta^{AA}/\zeta^{CG} = S_{AA-UA}(M)S_{UA-CG}(M)[s/\tau]$, we then determine long chain polymer diffusion constants and compare these to experiment.

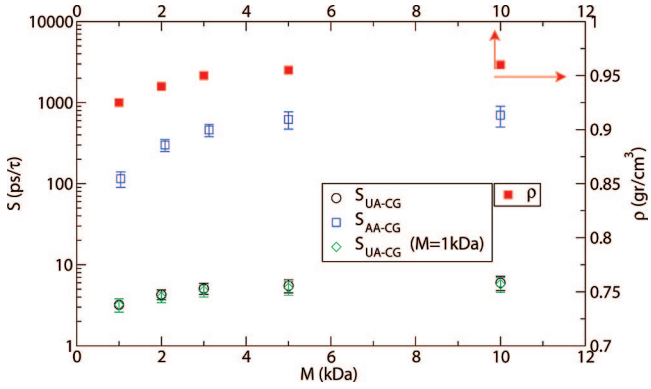

Figure 5. Time mapping of the CG simulations of the PS melts, using UA (circles) and AA (squares) data, and density, ρ (filled squares), as a function of M ($T = 463$ K). With diamonds are the time mapping of the CG simulations using UA data of 1 kDa melt at different densities. Diamonds and circles are almost indistinguishable.

Figure 5 shows S_{UA-CG} (circles) for the systems studied by both UA MD and CG MD simulations. As we can see, S_{UA-CG} varies in the short length regime (up to about 50 monomers), ranging from 3.1 ps/τ to about 6.0 ps/τ, and then it remains constant. This is in phase with the observed change in density, which varies from 0.925 g/cm^3 for 1 kDa to about 0.97 g/cm^3 for the 10 kDa and higher molecular weight melts.[61,66] At high molecular weights (above 10 kDa) the change in the polymer dynamics is entirely due to the increase of the molecular weight. On the other hand, in the short length regime the changes in the friction coefficient, and thus in the dynamics, are both due to the local polymer conformations and to the change of the density (chain end free volume effect). The dependence of the friction coefficient on density is not described accurately with the CG model, resulting into a dependence of S on the density (and on the molecular length).

The important result of Figure 5 is that a single value for the time scaling parameter S is appropriate to describe the dynamics of long polymer chains. S_{AA-CG} is shown in Figure 5 with squares and exhibits a qualitatively similar dependence on M as S_{UA-CG}; i.e., it varies in the low M regime (up to about 50 monomers) and then it approaches a constant value. However, S_{AA-CG} values are about 30−100 times larger than the S_{UA-CG} ones. Alternatively, one can follow the observation that the variation of S follows approximately the changes in density rather than the molecular weight itself, even though this density change is due to the chain length variation. Therefore, by performing the time mapping for the short chain system but at the density of the longer chains, one also can obtain a reliable estimate of S_{AA-UA}. If we follow this procedure, the combined time mapping $S_{AA-CG}(M) = S_{AA-UA}(M)S_{UA-CG}(M)$ varies between $\simeq$100 ps/τ (for the 1 kDa system) and $\simeq$700 ps/τ for the high (10 kDa and above) molecular weight (polymeric) regime. The underlying assumption in this procedure is that two melts which have the same density are also dominated by the same monomeric friction coefficient, at fixed temperature. This is justified if we consider that in polymers melts the average free volume in the system, f, varies with molecular weight as $f(M) = f_\infty + A/M$, where f_∞ is the free volume of infinite molecular weight polymer and A is a constant dependent on the chemistry. The corresponding expression for the density is $\rho(M) = (1/\rho_\infty + A/M)^{-1}$. More importantly, the friction coefficient, ζ, at fixed temperature, follows

$$\zeta(M) = \zeta_\infty \exp(B(1/f(M) - 1/f_\infty)) \qquad (2)$$

with ζ_∞ the friction coefficient of infinite molecular weight.[1] This means that if two systems have the same free volume (or density), then they should be characterized by the same monomeric friction coefficient. In order to check this hypothesis, we also perform a few UA MD simulations for the 1 kDa melt at the density of the longer chains. The results for the $S_{UA-CG}(M = 1$ kDa) are also shown in Figure 5 (diamonds). As we can see, the agreement with the $S_{UA-CG}(M)$ data from the time mapping using UA MD simulations of the longer systems (circles in Figure 5) is very good; i.e., data are almost indistinguishable. Furthermore, the friction coefficient aggregates contributions from the local structure in the melt. Our CG model would be expected to describe these contributions, since it has been developed through a methodology which ensures that the local structure is described accurately.[13,17] For the 1 kDa system used here the density deviates only 4−5% from high molecular weight systems, changing the local distances only by about 1%. This small change, as mentioned above, does not alter the typical local structure of the polymer melt, also because we are far away from any possible phase transition.

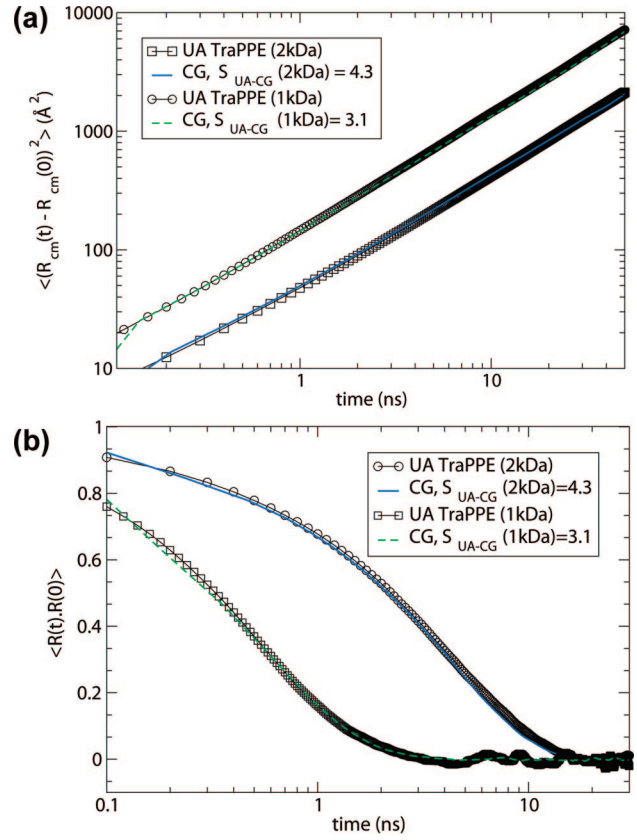

Figure 6. Time mapping of the CG simulations using united-atom atomistic data for two PS melts ($M = 1$ and 2 kDa, $T = 463$ K) based on the motion of the whole chain through (a) mean-square displacement of the chain center of mass and (b) end-to-end vector autocorrelation function.

The asymptotic plateau value of $S(M)$ can be used for scaling the CG dynamic results of much longer polymeric chains, where it is not possible to have reliable atomistic data. This allows us to quantitatively predict the diffusion coefficient of higher molecular weight PS melts directly from the CG simulations *without any adjustable parameter*.

Next we examine how $S(M)$ depends on translational and orientational dynamical modes of the polymeric chains. This is an important issue since it is directly related with the more general aspect concerning the validity and the transferability of the CG models to different conditions. Figure 6a shows the mean-square displacements of chain center of mass, $g_3(t)$ ($g_3(t) \equiv \langle(R_{cm}(t) - R_{cm}(0))^2\rangle$), from the UA MD and the CG MD simulations for two specific PS melts (1 and 2 kDa both at $T =$

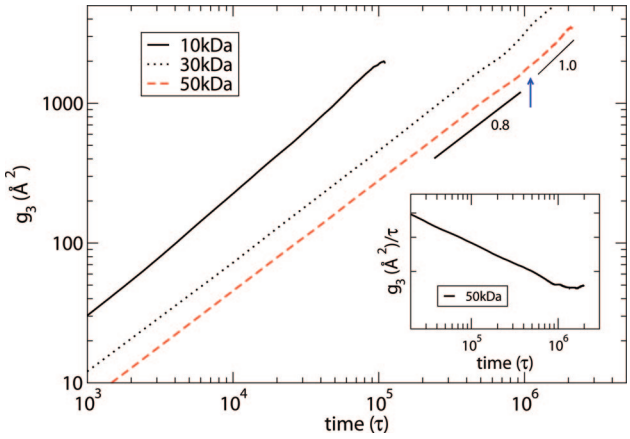

Figure 7. Mean-square displacement of the chain center-of-mass, g_3, for various PS melts ($T = 463$ K). In the inset g_3/t for the 50 kDa melt is shown.

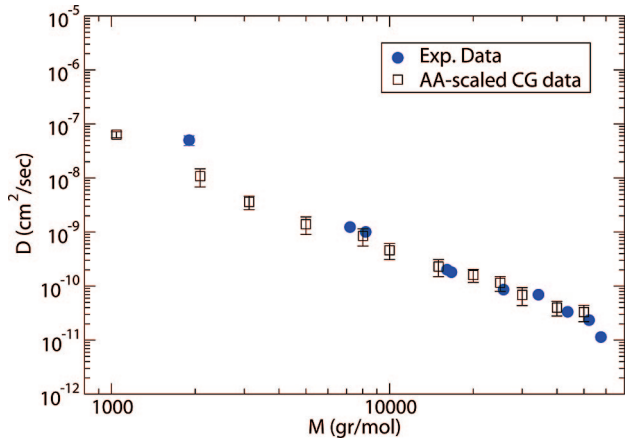

Figure 8. Self-diffusion coefficient of PS melts as a function of the molecular weight obtained from CG MD simulations (squares) and experiments (circles)[41] ($T = 463$ K).

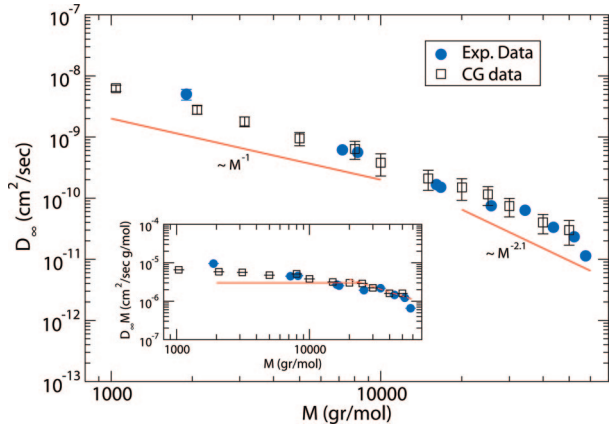

Figure 9. Self-diffusion coefficient of PS melts, after correcting for the chain length dependent friction coefficient, $D_\infty M$, as a function of the molecular weight. In the inset $D_\infty M$ vs M is shown ($T = 463$ K).

463 K). The scaling factor, S_{UA-CG}, obtaining by overlapping the two curves in the long time (Fickian) regime gives the CG time unit, i.e., $S_{UA-CG} = D^{CG}/D^{UA}$. For these two systems we have $S_{UA-CG} = 3.1$ (1 kDa, $T = 463$ K) and $S_{UA-CG} = 4.3$ (2 kDa, $T = 463$ K).[93] It is remarkable that both sets of curves follow exactly each other for distances above only 4−6 Åand for times above a few hundred picoseconds. The possibility to describe accurately the motion of a PS chain at such small length and short time scales is one of the advantages of the present CG model and is directly related to the fact that the model was chosen such as to be close to the atomistic structure.

Figure 6b shows the end-to-end vector autocorrelation function, $\langle R(t)\cdot R(0)\rangle/\langle R^2\rangle$, from the UA and CG MD simulations, for the two PS melts shown in Figure 6a. The rescaled factor is again $S_{UA-CG} = 3.1$ (1 kDa, $T = 463$ K) and $S_{UA-CG} = 4.3$ (2 kDa, $T = 463$ K); i.e., the time mapping is exactly the same with the one derived from the msd of the chain center of mass. Similar to Figure 6a, both curves follow exactly each other for times above a few hundred picoseconds. Thus, our CG model describes correctly both the translational and the orientational dynamics of the PS melts as predicted by the UA simulations. Also, for the other PS melts studied here the picture is similar. Note also that the time mapping is the same if a dynamical quantity describing the segmental dynamics (like the mean-square displacement of the CG beads) is used.[52] Finally, a detailed investigation of the dependence of both structure and dynamics of CG PS melts on the tacticity (fully stereoregular vs atactic PS melts) is currently in progress.[67]

In summary of the discussion above, we can also provide a crude estimate of the overall speed-up compared to detailed all-atom MD simulations. A time unit τ of about 700.0 ps results in a time step for the integration of equations of motion more than 3 orders of magnitude larger than a typical time step used in the all-atom MD simulations. Taken also into account the smaller number of beads describing a PS chain, i.e., each PS monomer corresponds to two CG beads compared to 16 in the all-atom, the overall efficiency of the model, or the speed-up that can be achieved, is more than 4 orders of magnitude. In practice, the actual speed-up is even larger because of the simpler and shorter ranged nonbonded CG interaction potential compared with the atomistic one. In addition, in the mesoscopic description it is much easier to obtain well-equilibrated chains of high molecular weight compared to the atomistic one.

5. Dynamics of Polystyrene Melts

5.1. Self-Diffusion Coefficient. Figure 7 shows the mean-square displacement of the chain center-of-mass obtained directly from the CG MD simulations as a function of time (in τ units) averaged over all chains in the system:

$$g_3(t) = \langle(\mathbf{R}_{cm}(t) - \mathbf{R}_{cm}(0))^2\rangle \tag{3}$$

Three different atactic PS melts with 10, 30, and 50 kDa molecular weight are presented in Figure 7. All systems exhibit a qualitatively similar behavior: In the small time regime (times shorter than the longest relaxation time) a well-known non-Fickian subdiffusive behavior, related to the correlation hole cage effect, is observed, where $g_3 \propto t^{0.8}$.[4,8,12] In the longer time regime the standard linear Fickian regime is observed. For example, for the 50 kDa PS melt the arrow marks roughly the two different regimes; i.e., g_3 for times up to about $10^6\tau$ can be fitted with an exponent of about 0.8 whereas longer times with an exponent of about 1. This is more clear in the inset of Figure 7 where $g_3(t)$ scaled with time, for the 50 kDa PS melt, is shown.

From the linear part of $g_3(t)$ curves, the self-diffusion coefficient, D, can be obtained through the Einstein relation:

$$D = \lim_{t\to\infty} \frac{g_3(t)}{6t} \tag{4}$$

Figures 8 and 9 present predictions for the self-diffusion coefficient, D, of the atactic PS melts as a function of the molecular weight, M, obtained from the CG MD simulations. Our goal is to examine the ability of the CG simulations to

predict quantitatively the polymer diffusion by comparing the CG PS self-diffusion predictions with experimental data. Therefore, we scale the CG "raw" data, using the time mapping factor, S, found in the previous section and calculate D in units of cm^2/s. Diffusion coefficients obtained from the CG simulations, scaled with the time mapping factor taken from the all-atom MD simulations, S_{AA-CG}, are shown in Figure 8 with squares. In the same figure experimental data for the self-diffusion of PS melt (diffusion of a polymer chain in a matrix with the same molecular weight)[38,41] are presented with circles. The experimental data are corrected for the slightly different temperature ($T = 458$ K) with the temperature dependence reported in ref 41. Note that both simulation and experimental data are not corrected for the chain end free volume, i.e., the chain length dependence of the glass transition temperature. As we can see, the AA-scaled CG data are in very good agreement with the experimental data, especially in the high molecular length regime. This is of particular importance if we consider that results from the CG dynamic simulations are compared to experimental data by using only detailed atomistic simulations for a few short-chain reference systems, *without any adjustable parameter*. The larger deviation between the simulation and the experimental data in the short length regime is not surprising if we consider the effect of the (small) polydispersity of the experimental data ($I \simeq 1.04$): in these short chains the presense of even only a few PS oligomers can increase the diffusion constant of the polymers in these systems. Finally, note that scaling the CG data with the time mapping factor obtained from the UA TraPPE MD simulations would lead to deviations of more than 1 order of magnitude, giving wrong results.

Of additional interest is the molecular weight dependence of self-diffusion coefficient D. Both AA-scaled CG simulation and experimental data in Figure 8 can be fitted using a power-law dependence ($D \sim M^{-b}$) for the entire region of molecular weights studied here using a power-law dependence ($D \sim M^{-b}$) with an exponent $b \approx 2.1 \pm 0.2$.[41] This dependence is also in agreement with other experimental measurements of self-diffusion coefficient of atactic PS melts at different temperatures ($T = 498$ K), where it has been shown that D scales with M as about $D \sim M^{-2}$ for molecular lengths below and above the characteristic molecular weight for the formation of entanglements, M_e.[37,40] From the point of view of the theory different exponents are predicted for short unentangled chain polymer melts (the Rouse model predicts $b = 1$) and for the longer entangled polymer melts ($M > M_e$), for which the reptation theory predicts $b = 2$. However, the Rouse model neglects the chain length dependent molecular friction coefficients which, for the low molecular weight regime, dominate system dynamics and accelerate polymer diffusion.[1,73] This effect can be directly eliminated in the simulation data if they are corrected using the time mapping of the high molecular weight regime, i.e., if all CG data are scaled with the plateau value of $S_{AA-CG}(M)$. For the experimental data a correction can be made in D using data about the temperature and molecular weight dependence of friction coefficient (or free volume).[40,41] In more detail D is assumed to obey the free volume expression

$$D = D_\infty(M) \exp(-B(1/f(M,T) - 1/f_\infty(T))) \quad (5)$$

where $f(M,T)$ is the free volume of the system, which depends on M and temperature, and $f_\infty(T)$ is the free volume of a matrix with $M \rightarrow \infty$ at temperature T. $D_\infty(N)$ is the corrected diffusion coefficient, and B is a constant that can be calculated using data about the temperature dependence of self-diffusion coefficient. Equation 5 underlies the WLF equation.[1] The free volume $f(M,T)$ can be calculated according to

$$f(M,T) = f_g + \alpha(T - T_g(M)) \quad (6)$$

where f_g is the free volume at the glass transition temperature, T_g. Values about f_g, the temperature coefficient α, the molecular weight dependent $T_g(M)$, and the constant B have been obtained from the literature.[1,40] This procedure has been used for the experimental data.

New values of self-diffusion coefficient of atactic PS melts, $D_\infty(M)$, for both CG simulation and experimental data are shown in Figure 9. AA-scaled CG simulation data are shown with squares while experimental data with circles. The agreement between the two sets of data shows that the applied corrections also agree. As we can see, the chain end free volume correction affects only the small N_{mon} regime ($N_{mon} < 200$). In this regime AA-scaled CG D data follow a power-law dependence $D_\infty \sim M^{-b}$ with $b \approx 1.2 \pm 0.2$. This exponent is very close to the one predicted by the Rouse model ($b = 1$). Experimental data follow a similar dependence with slightly larger exponent, $b \approx 1.5 \pm 0.2$. Data in the second regime are not affected by the above correction, and the power law exponent remains $b \approx 2.1 \pm 0.2$. According to the original reptation theory, the latter exponent is 2.[2] However, phenomena such as the contour length fluctuations (CLF) and constraint release (CR) typically accelerate the escape of the chain from the tube, causing an increase in D. A recently proposed theory that incorporates CLF and CR phenomena predicts a stronger exponent between 2.1 and 2.4.[73] This stronger exponent has been also observed in recent studies of various polymers.[42] In addition, atomistic MD simulations of polyethylene[8,9] and polybutadiene[10] show an exponent of about 2.3 for slightly entangled melts.

The molecular weight for the crossover from Rouse to reptation-like behavior, M_e, from our CG diffusion data, corrected for the chain end free volume (see also inset in Figure 9 where $D_\infty M$ vs M is shown), is around 25 000−30 000 g/mol, i.e., $N_e \approx 240-300$ monomers. This is in good agreement with the experimental data, from forced Rayleigh scattering measurements (circles in Figure 9), which show a transition regime in the range of molecular weights of about 30 000−35 000 g/mol, i.e., $N_e \approx 288-335$.[38] Experimentally, it has been also reported that the crossover is shifted from a value of $M_e \approx 18\,000$ g/mol for the diffusion of PS melts in a high molecular weight matrix to a value of $M_e \approx 33\,000$ g/mol for the diffusion of PS melts in matrix with the same molecular weight (self-diffusion data).[41]

We should also mention here that in two recent works using alternative CG models of PS[18,20] smaller values for N_e, of about 80−100 monomers, obtained from self-diffusion data, at $T = 503$ K[18] and $T = 450$ K[20] were claimed. Both values are relatively small compared to the value predicted from our CG simulations and to experimental data of the same quantity. In both these works chain lengths only up to about 200 monomers were studied, and it is also not clear whether the data were corrected for the density effect.

Note also that the self-diffusion coefficient of the higher molecular weight entangled PS melts studied here (50 kDa) is of the order of about 10^{-11} cm^2/s. This results in relaxation times, on the level of the end-to-end vector, τ_d (according to reptation theory $\tau_d = \langle R^2 \rangle / 3\pi^2 D^2$), of about 6.0 ms, many orders of magnitude longer that what can be modeled with detailed atomistic molecular dynamic simulations in such systems.

Finally, as a general remark, it is clear from Figure 8 that the level of quantitative agreement between the CG predictions and the experimental data depends on both the atomistic and the CG model and, of course, on the quality of the experiments. Even if the CG model is capable of reproducing *qualitatively* well the dynamics of the specific polymer, the use of an accurate atomistic model is of great importance in order to predict *quantitatively* the dynamics of polymer chains. However, the clear advantage of the hierarchical methodology, which combines atomistic and CG dynamic simulations, is that with the

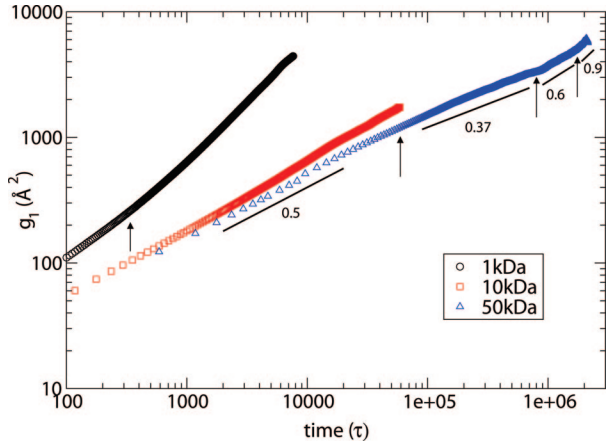

Figure 10. Mean-square displacement of the innermost segments vs time for different CG PS melts studied here ($T = 463$ K).

latter we are able to extend many orders of magnitude the range of molecular weights, as well as the length and time scales that can be studied, compared to brute force atomistic ones. Furthermore, our simulations also support the experiments since both are completely independent.

5.2. Mean-Square Displacement of Chain Segments. The dynamics of the different systems can also be studied through the calculation of the mean-square displacement of the segments averaged over all beads i:

$$g_1(t) = \langle(\mathbf{r}_i(t) - \mathbf{r}_i(0))^2\rangle \tag{7}$$

where g_1 represents the msd for the individual bead i of each chain.

According to the Rouse model,[2] for unentangled systems, the g_1 is calculated to be

$$g_1 = 6Dt + \frac{4\langle R^2\rangle}{\pi^2}\sum_{p=1}^{\infty}\frac{1}{p^2}\cos\left(\frac{p\pi i}{N}\right)^2[1 - \exp(-tp^2/\tau_R)] \tag{8}$$

where the sum is over all normal modes, $\tau_R = \zeta N\langle R^2\rangle/3\pi^2 k_B T$ is the Rouse time, and ζ is the monomeric friction coefficient. For very short times g_1 is dominated by the terms with large p and scales as $t^{1/2}$. On the other hand, for longer times ($t \gg \tau_R$), the second term in the above equation can be neglected and g_1 scales as t.

The msd of the chain segments according to the reptation theory is much more complicated. In more detail, g_1 exhibits four different power law regimes:[2]

$$g_1(t) \sim \begin{cases} t^{1/2}, & t \le \tau_e \\ t^{1/4}, & \tau_e \le t \le \tau_R \\ t^{1/2}, & \tau_R \le t \le \tau_d \\ t, & \tau_d \le t \end{cases} \tag{9}$$

where $\tau_e \propto N_e^2$ is the entanglement time (time at which the segmental displacements becomes comparable to the tube diameter). The predicted $t^{1/4}$ scaling is a consequence of two effects: the Rouse-like diffusion and the tube constraints. Finally, $\tau_d \propto N^3/N_e^2$ is the disentanglement time. In the long-time regime ($t \ge \tau_d$) the dynamics is governed by the overall diffusion of the chain, and g_1 follows the Fickian linear dependence.

Figure 10 shows plots of g_1 of the segments for various chain lengths. In this graph we average only over the innermost (about 20) segments in the chain, which experience the topological constraints from the environment more strongly. Three different curves are shown, corresponding to 1, 10, and 50 kDa PS melts.

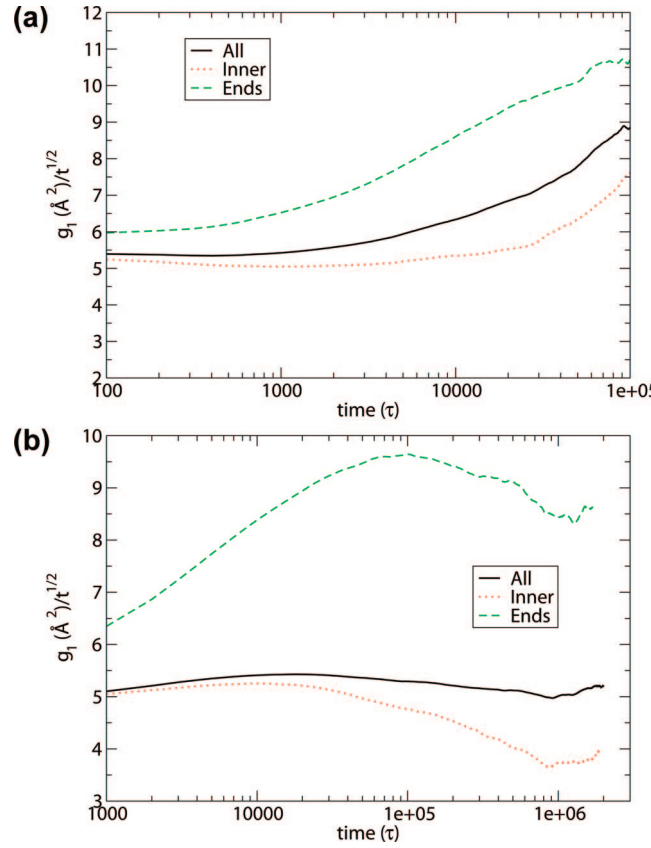

Figure 11. Mean-square displacement of the segments normalized by the Rouse slope of $t^{1/2}$ for different PS melts (a) 10 kDa and (b) 50 kDa.

The circles refer to the PS 1 kDa melt and are clearly seen to be in good agreement with the predictions of the Rouse model: in the short-time regime (marked by the arrow) $g_1 \propto t^{1/2}$, and in the long-time (Fickian diffusion) $g_1 \propto t^1$. In fact, due to the non-negligible contribution of the linear term in eq 8 in this time scale, the slope of the short-time time is slightly higher than 0.5, close to 0.6.

Also shown in Figure 10 are the curves corresponding to 10 kDa (squares) and to 50 kDa (triangles) PS melts. The 10 kDa line corresponds to a system in the transition regime from Rouse-like to reptation behavior and do not show any pronounced structure. In contrast, the 50 kDa system shows three breaks (marked by arrows) characteristic of a system exhibiting reptation-like dynamics. The corresponding effective exponents are equal to 0.5, 0.37, and 0.6. However, the different regimes are not clearly separated as expected for the molecular weights studied here. The differences from the predictions of the reptation theory (mainly for the intermediate regime with the $t^{1/4}$ behavior) are expected since these power laws are valid in the long chain length regime only.[74,75]

The deviations from the Rouse behavior can be seen more clear if g_1 is calculated for segments in various positions along the chain, scaled with the Rouse slope $t^{1/2}$. Figures 11a,b show $g_1/t^{1/2}$ vs time (in τ units) calculated as an average over all segments as well as for the innermost and the outermost (ends) segments, for the 10 and 50 kDa PS melts. Plateau-like regimes are signals of Rouse behavior, whereas regimes with negative slope in intermediate times are indications of entanglement constraints. The long times correspond to the linear diffusion; i.e., the slope of g_1 is about 1. As expected, a different behavior between innermost and outermost segments is observed. Outermost segments move faster (due to the higher mobility of chain ends) for short and intermediate times. For very long times end

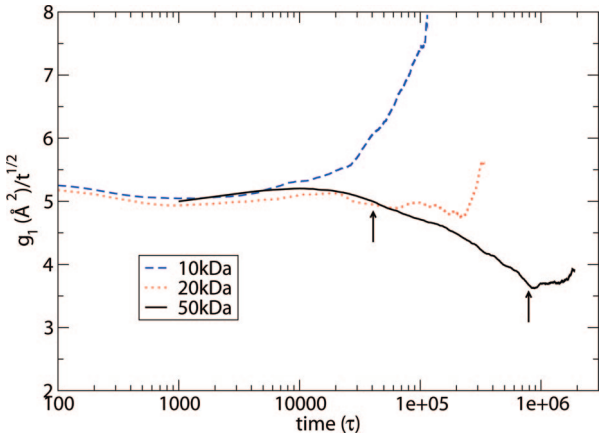

Figure 12. Mean-square displacement of the innermost segments normalized by the Rouse slope of $t^{1/2}$ for different PS melts.

segments slow down due to the connectivity with the other segments. This is more clear for the higher molecular weight melts (50 kDa, Figure 11b), where topological constraints of the innermost segments are stronger.

More importantly, there is a clear different behavior between the innermost segments of the two PS melts shown in Figures 11a,b. The innermost segments of the 10 kDa melt do not show any signals of negative slope; i.e., slope of $g_1/t^{1/2}$ changes gradually from a plateau Rouse-like regime to the linear one. In contrast, the dynamics of the innermost segments of 50 kDa is qualitatively different: $g_1/t^{1/2}$ shows a reptation-like regime with negative slope, in agreement with Figure 10, for times between $4 \times 10^4\tau$ and about $0.8 \times 10^6\tau$. For longer times up to about $1.5 \times 10^6\tau$ there is again a plateau-like regime (third region in reptation behavior), and then for the longer times the standard linear regime starts to appear. Note the rather short time range of the second plateau regime. This is not surprising if we consider that even the higher molecular weight PS melt studied here (50 kDa) is rather a mildly entangled one, and therefore its reptation time is of the same order with its Rouse time.

The deviations of the dynamics of innermost segments form the Rouse behavior, for the various molecular weights, are shown in Figure 12. There is a clear crossover regime from unentangled (Rouse-like) to entangled (reptation-like) behavior for the molecular weights in the range from 20 to 50 kDa. Another interesting aspect is the estimation of N_e from segment displacements. To use directly the different crossover times in g_1 (see eqs 9) is not straightforward because prefactors involve the friction coefficient, ζ. Furthermore, τ_d, as also the zero-shear rate viscosity η_0, is known to follow a $N^{3.4}$ power law rather than the predicted N^3 due to a very slow crossover to the asymptotic regime.[1] A rather crude estimate of N_e can be obtained by taking the ratio between the entanglement and the Rouse time, i.e., $\tau_e/\tau_R = N_e^2/N^2$. Using the data for the longest PS melt studied here, $M = 50$ kDa (marked by arrows in Figure 12), we get an estimate of $N_e \simeq 110 \pm 30$ monomers. Note the high error bar in the above value, which is due to the crude estimate of the intermediate characteristic time. Indeed, as is obvious from the data shown in Figure 12, for the accurate estimation of both τ_e and τ_R higher molecular weight systems are needed, as has been also discussed elsewhere.[34,74] This will be a part of a future work.

6. Primitive Path (Entanglement) Analysis

Mapping the CG MD data onto the reptation model is a subtle task because reptation theory has been formulated in terms of chain primitive paths (PP), through an appropriate coarse-graining of the real chain. The link between the real chain and the primitive paths has been established in a recently developed topology analysis, which allows to determine the primitive path of the chains and thus N_e.[76−78] There it has been shown that the average length of this primitive path and the corresponding N_e are in good agreement with the plateau modulus obtained from experimental measurements for a variety of systems including polycarbonate.[68] Later various alternative methods for obtaining primitive paths out of more realistic polymer chains have also been developed.[79−84] Here we follow the same procedure to obtain PPs as in refs 76 and 77 for the PS melts studied through our CG simulations. Overall, the whole methodology involves the following steps: First, the chain ends are fixed in space. Then the intrachain interactions (excluded-volume as well as bending and dihedral interactions are switched off), whereas all the interchain excluded-volume interactions are retained. Bonded CG beads interact only through a finite extensible nonlinear elastic (FENE) potential:

$$U_{\mathrm{FENE}} = -(kR_0^2/2)\log(1 - r^2/R_0^2) \tag{10}$$

where k is the spring constant and R_0 is the maximum extension of the FENE bond. This potential has a minimum at $r = 0$. We use a value of $k = 30\epsilon/\sigma^2$ and $R_0 = 1.5\sigma$. Then the energy of the system is minimized by slowly cooling the system to $T = 0$ K. During the cooling procedure we use a time step of $\Delta t = 0.005\tau$. The systems are equilibrated to ensure that the topological state of the network of the chain primitive paths is not altered. To ensure this, we continuously monitor the bond lengths and the total energy. Finally, as shown elsewhere,[77] to the present level of accuracy the effect of the self-entanglements can be neglected. More details about the algorithm can be found elsewhere.[76,77]

The above-described primitive path analysis (PPA) has been applied to all CG PS melts studied in this work. Figures 13a,b show a representative CG configuration for the 50 kDa PS melt as well as the mesh of primitive paths obtained out of it. As shown in Figure 13b, the resulting PPs consist of short chain segments of strongly fluctuating length and sharp turns at entanglements points between two paths. The end-to-end distance of the original chain, $\langle R^2(N)\rangle$, and the corresponding primitive path one

$$\langle R_{\mathrm{pp}}^2(N)\rangle = \alpha_{\mathrm{pp}}\langle L_{\mathrm{pp}}\rangle \tag{11}$$

are the same. Thus, the above procedure directly leads to the Kuhn length of the primitive paths α_{pp}; i.e., $\alpha_{pp} = \langle R^2(N)\rangle/\langle L_{pp}\rangle$ with $\langle L_{pp}\rangle$ being the PP contour length, calculated as an ensemble average over all present chains. This determines the entanglement length, N_e (in number of monomers), via

$$N_e = \alpha_{\mathrm{pp}}^2 N_{\mathrm{mon}}/\langle R^2(N)\rangle \tag{12}$$

where N_{mon} is the number of monomers per chain. Figure 14 shows the entanglement length N_e, obtained from the primitive path analysis, as a function of N_{mon}. As we observe N_e gradually increases as the chain length increases, until it approaches an asymptotic value. The estimated value of the longer melts is about 205 ± 30 monomers. This leads to an entanglement molecular mass M_e of about 21 000 g mol^{-1}. Experimentally reported values are between 13 000 and 18 000 g/mol.[40,85,86] Recent rheological measurements of the plateau modulus, G_N^0, of various molecular weight samples, estimate a value of about $(1.95 \pm 0.2) \times 10^5$ Pa at $T = 423-433$ K.[86] This leads for M_e ($M_e = 4\rho RT/5G_N^0$) to a value of about $14\,500 \pm 1000$ g/mol or $N_e \approx 140 \pm 10$ at $T = 423$ K. The packing length p, which depends on the number density of the polymer chains and the

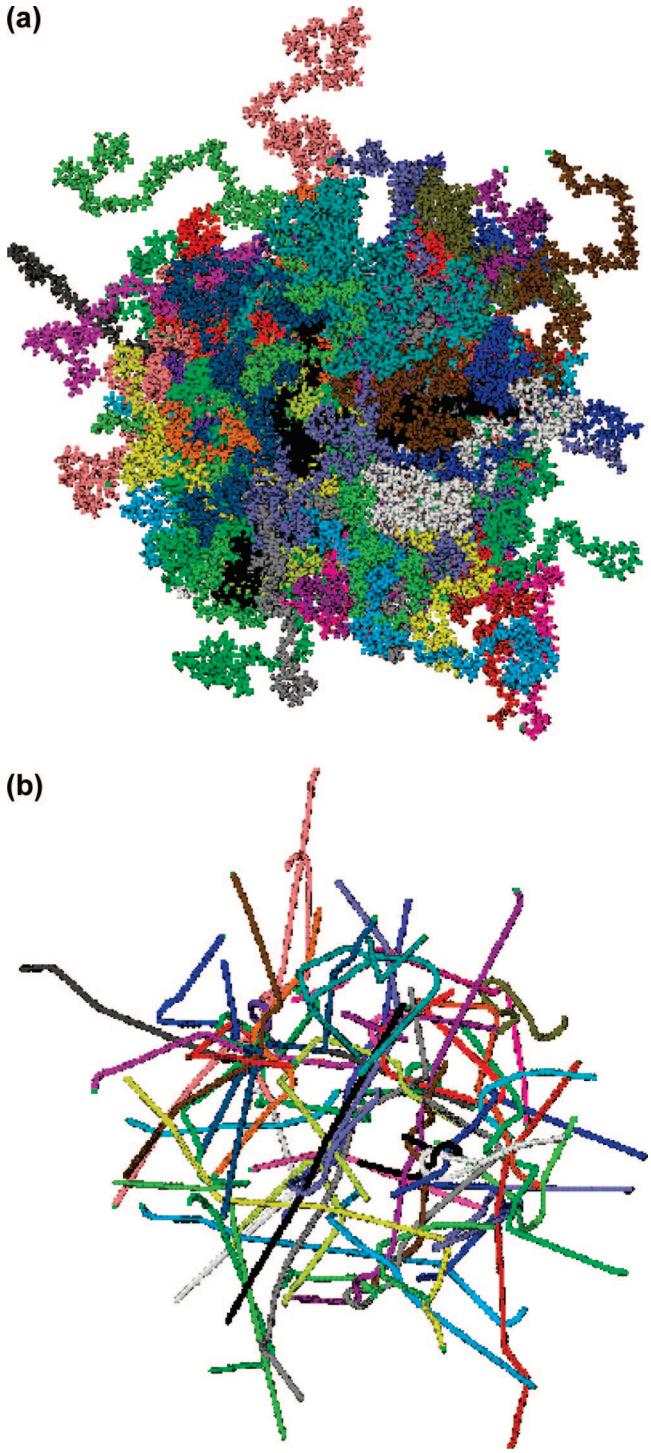

Figure 13. (a) Representative CG PS melt sample and (b) corresponding PP network for the PS 50 kDa melt. Each chain is shown with a different color.

chain dimensions ($p = M/\langle R^2\rangle \rho N_A$), is about 4.6 ± 0.4 Å. The experimental value is 3.95 Å at a lower temperature ($T = 413$ K).[85] The difference between the simulation and the experimental values is due to the different temperature (as the temperature increases p also increases since both density and $\langle R^2\rangle$ decreases) and because of the slightly smaller value of C_N predicted by the CG simulations. If we consider that $M_e \propto p^{-3}$,[85] then this difference is also consistent with the slightly larger value of M_e estimated from our CG simulations compared to the experimental one.

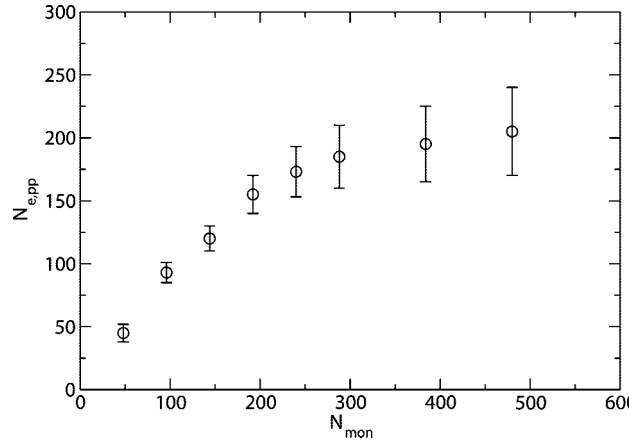

Figure 14. Entanglement length N_e, in monomers, obtained from the primitive path analysis, as a function of chain length N_{mon} ($T = 463$ K).

7. Discussion and Conclusions

In the present work, a detailed study of the dynamics of PS melts through a computational approach that combines atomistic and CG dynamic simulations has been presented. A recently proposed CG PS model, which allows for much larger systems and significantly longer times, compared to atomistic MD simulations, has been used. First the dynamics of the CG PS melts has been compared with detailed atomistic data by using a proper time mapping scaling parameter, $S(M)$, based on results of short PS chains. The parameter $S(M)$ has been computed and found to be consistent, using data from translational (mean-square displacements of chain center-of-mass and of segments) as well as orientational (autocorrelation function of the end-to-end vector) dynamics. Following a hierarchical approach that combined atomistic, united atom, and CG simulations, the molecular weight dependence of $S(M)$ can be accurately calculated. The plateau value of S can be used for scaling the CG dynamic results of longer polymeric chains, where it is not possible to have reliable atomistic data. Thus, we are able to calculate for the first time dynamical properties of high molecular weight entangled PS melts and to compare directly with experimental data.

CG self-diffusion coefficients, scaled with atomistic data, found in very good quantitative agreement with the experimental measurements. Furthermore, both simulation and experimental data show, after correcting for the chain end free volume, a clear transition regime from Rouse to reptation-like behavior. The molecular length for the crossover from Rouse to reptation-like behavior, N_e, from our CG diffusion data, is around $N_e \approx 240-300$ monomers in good agreement with experimental data. The MSDs of segments have also been calculated. For the short systems ($M = 1$ kDa) data were found in good agreement with the Rouse predictions, whereas for the longer systems ($M = 50$ kDa) three different regimes with exponents close to the predictions of the reptation theory are observed. The simulated systems were also analyzed in the level of primitive paths, and the entanglement molecular length, N_e, has been obtained.

All the values for the entanglement molecular length N_e of PS (in number of monomers), obtained from different simulation and experimental methods, are reported in Table 3. A few interesting points are arising here. First both simulation and experimental values of N_e obtained from self-diffusion data ($N_e \simeq 240-300$) are clearly larger than the one reported by rheological measurements ($N_e \simeq 140-180$). This is not surprising: a similar tendency has been also observed for polyethylene[9,87] and for polycarbonate.[68] Second, N_e determined from the modulus is larger than the one coming from the bead

Table 3. Entanglement Molecular Length (in Number of Monomers), N_e, of Atactic PS Melts Obtained from Various Experimental and Simulation Methods

method	temp (K)	N_e	ref
rheology (plateau modulus G_N^0)	423	140 ± 10	86
self-diffusion coefficient	458	280−320	41
self-diffusion coefficient	463	240−300	this work
self-diffusion coefficient	503, 450	80−100	18, 20
segmental dynamics	463	110 ± 30	this work
entanglement analysis (PPA)	463	205 ± 20	this work
entanglement analysis (CRETA)	413	124	26

displacements (segmental dynamics), in agreement with previous studies using simple bead spring models with variable flexibility.[74] The values of N_e calculated from the different methods are consistent, within the error bars, and in good agreement with experimental data. Overall, the great spread for the different estimates of the entanglement molecular length N_e, reported in Table 3, is of importance. The deviations are within a factor of 3. This shows that the determination of N_e based on different experimental quantities than the plateau modulus will lead to different values. This is of particular importance when analyzing and comparing results from different experimental techniques. Furthermore, the data emphasize the fact that there is not a well-established theory, especially in the crossover regime from Rouse-like to reptation-like behavior, which for polystyrene (PS) covers a range of molecular weights from about $M \approx 1$ kDa to $M \approx 50$ kDa.

Recently, we also observed that data about the diffusion of ethylbenzene molecules dissolved in PS matrix obtained from CG simulations, scaled with UA data, were in semiquantitative agreement with experimental data.[53] Following the approach proposed here, and scaling the CG data with all-atom dynamic data, the results for the dynamics of EB are in much better agreement with experimental data; this will be a part of a future work.

Future plan also concerns the implementation of the current CG models to polymer/solid interfacial systems. There CG models can be directly incorporated in multiscale methodologies, which include multiple levels of simulations at the same time, were both atomistic, and mesoscopic descriptions are needed.[88,89] This is important since for the study of the long-time dynamics of polymers in such systems an atomistic description needed very close to the surface whereas a mesoscopic description can be used for length scales far from the surface.[90−92]

Acknowledgment. Very fruitful discussions with Vakhtang Rostiashvili, Nico van der Vegt, Dominik Fritz, and Dirk Reith are greatly appreciated. V.H. acknowledges financial support by the German Research Foundation under Grant SFB 625.

References and Notes

(1) Ferry, J. D. *Viscoelastic Properties of Polymers*; John Wiley and Sons: New York, 1980.
(2) Doi, M.; Edwards, S. F. *The Theory of Polymer Dynamics*; Claredon Press: Oxford, England, 1986.
(3) Mcleish, T. *Adv. Phys.* **2000**, *51*, 1379.
(4) *Monte Carlo and Molecular Dynamics Simulations in Polymer Science*; Binder, K., Ed.; Oxford University Press: New York, 1995.
(5) Baschnagel, J.; Binder, K.; Doruker, P.; Gusev, A. A.; Hahn, O.; Kremer, K.; Mattice, W. L.; Müller-Plathe, F.; Murat, M.; Paul, W.; Santos, S.; Suter, U. W.; Tries, V. *Adv. Polym. Sci.* **2000**, *152*, 41.
(6) Kremer, K. In *Proceedings of the International School of Solid State Physics - 34th Course: Computer Simulations in Condensed Matter: from Materials to Chemical Biology*; Binder, K., Ciccoti, G., Eds.; Erice, 2006.
(7) Kremer, K.; Grest, G. S. *J. Chem. Phys.* **1990**, *92*, 5057.
(8) Harmandaris, V.; Mavrantzas, V. Molecular Dynamic Simulations of Polymers. In *Simulation Methods for Polymers*; Theodorou, D. N., Kotelyanski, M., Eds.; Marcel Dekker: New York, 2004.
(9) Harmandaris, V.; Mavrantzas, V.; Theodorou, D. N.; Kröger, M.; Ramirej, J.; Öttinger, H.; Vlassopoulos, D. *Macromolecules* **2003**, *36*, 1376.
(10) Tsolou, G.; Mavrantzas, V. G.; Theodorou, D. N. *Macromolecules* **2005**, *38*, 1478.
(11) Abrams, C.; Kremer, K. *Macromolecules* **2003**, *36*, 260.
(12) Paul, W.; Binder, K.; Kremer, K.; Heermann, D. *Macromolecules* **1991**, *24*, 6332.
(13) Tschöp, W.; Kremer, K.; Batoulis, J.; Buerger, T.; Hahn, O. *Acta Polym.* **1998**, *49*, 61; **1998**, *49*, 75.
(14) Reith, D.; Meyer, H.; Müller-Plathe, M. *Macromolecules* **2001**, *34*, 2335.
(15) Fukunaga, H.; Takimoto, J.; Doi, M. *J. Chem. Phys.* **2003**, *116*, 8183.
(16) Larson, R. G. *Mol. Phys.* **2004**, *102*, 341.
(17) Harmandaris, V. A.; Adhikari, N. P.; Van der Vegt, N. F. A.; Kremer, K. *Macromolecules* **2006**, *39*, 6708.
(18) Milano, G.; Müller-Plathe, F. *J. Phys. Chem. B* **2005**, *109*, 18609.
(19) Carbone, P.; Varzaneh, A. K.; Chen, X.; Müller-Plathe, F. *J. Chem. Phys.* **2008**, *128*, 064904.
(20) Sun, Q.; Faller, R. *Macromolecules* **2006**, *39*, 812.
(21) Haliloglou, T.; Mattice, W. L. *J. Chem. Phys.* **1998**, *108*, 6989.
(22) Li, X. J.; Kou, D. Z.; Rao, S. L.; Liang, H. *J. Chem. Phys.* **2006**, *124*, 204909.
(23) Padding, J.; Briels, W. J. *J. Chem. Phys.* **2002**, *117*, 925.
(24) Marrink, S. J.; De Vries, A. H.; Mark, A. E. *J. Phys. Chem. B* **2004**, *108*, 750.
(25) Nielsen, S. O.; Srinivas, G.; Klein, M. *J. Chem. Phys.* **2005**, *123*, 124907.
(26) Spyriouni, T.; Tzoumanekas, C.; Theodorou, D. N.; Müller-Plathe, F.; Milano, G. *Macromolecules* **2007**, *40*, 3876.
(27) Van der Vegt, N. F. A.; Peter, C.; Kremer, K. Structure-based coarse- and fine-graining in soft matter simulations. In *Coarse-graining of Condensed Phase and Biomolecular Systems*; Voth, G. A., Ed.; Chapmann and Hall/CRC Press, Taylor and Francis Group: **2008**.
(28) Luybartsev, A. P.; Laaksonen, A. *Phys. Rev. E* **1995**, *52*, 3730.
(29) Izvekov, S.; Parrinello, M.; Burnham, C. J.; Voth, G. A. *J. Chem. Phys.* **2004**, *120*, 10896.
(30) Praprotnik, M.; Delle Site, L.; Kremer, K. *Annu. Rev. Phys. Chem.* **2008**, *59*, 545.
(31) Murat, M.; Kremer, K. *J. Chem. Phys.* **1998**, *108*, 4340.
(32) Doi, M.; Takimoto, J. *Philos. Trans.: Math. Phys. Eng. Sci.* **2003**, *361*, 641.
(33) Likhtman, A. E. *Macromolecules* **2005**, *38*, 6128.
(34) Likhtman, A. E.; Sukumaran, S. K.; Ramirez, J. *Macromolecules* **2007**, *40*, 6748.
(35) Van den Noort, A.; den Otter, W. K.; Briels, W. J. *Europhys. Lett.* **2007**, *80*, 28003.
(36) Kindt, A.; Briels, W. J. *J. Chem. Phys.* **2007**, *127*, 134901.
(37) Bachus, R.; Kimmich, R. *Polymer* **1983**, *24*, 964.
(38) Antonietti, M.; Coutandin, J.; Sillescu, H. *Makromol. Chem., Rapid Commun.* **1984**, *5*, 525.
(39) Green, P. F.; Kramer, E. J. *Macromolecules* **1986**, *19*, 1108.
(40) Fleisher, G. *Colloid Polym. Sci.* **1987**, *265*, 89.
(41) Antonietti, M.; Fölsch, K. J.; Sillescu, H. *Makromol. Chem.* **1987**, *188*, 2317.
(42) Lodge, T. P. *Phys. Rev. Lett.* **1999**, *83*, 3218.
(43) Tao, H.; Lodge, T. P.; Von Meerwall, E. D. *Macromolecules* **2000**, *33*, 1747.
(44) Urakawa, O.; Swallen, S. F.; Ediger, M. D.; Von Meerwall, E. D. *Macromolecules* **2004**, *37*, 1558.
(45) Tirell, A. R. *Macromolecules* **1992**, *25*, 4605.
(46) Han, J.; Gee, R. H.; Boyd, R. H. *Macromolecules* **1994**, *27*, 7781.
(47) Mondello, M.; Yang, H.; Furuya, H.; Roe, R. *Macromolecules* **1994**, *27*, 3566.
(48) Lyulin, A. V.; Michels, M. A. J. *Macromolecules* **2002**, *35*, 1463.
(49) Lyulin, A. V.; Michels, M. A. J. *Phys. Rev. Lett.* **2007**, *99*, 085504.
(50) He, Y.; Luz, T. R.; Ediger, M. D.; Ayyagari, C.; Bedrov, D.; Smith, G. D. *Macromolecules* **2004**, *37*, 5032.
(51) Rapold, R. F.; Suter, U. W.; Theodorou, D. N. *Macromol. Theory. Simul.* **1994**, *3*, 19.
(52) Harmandaris, V. A.; Reith, D.; Van der Vegt, N. F. A.; Kremer, K. *Macromol. Chem. Phys.* **2007**, *208*, 2109.
(53) Harmandaris, V. A.; Adhikari, N. P.; Van der Vegt, N. F. A.; Kremer, K.; Mann, B. A.; Voelkel, R.; Weiss, H.; Liew, C. C. *Macromolecules* **2007**, *40*, 7026.
(54) Mulder, T.; Harmandaris, V. A.; Lyulin, A.; Van der Vegt, N. F. A.; Vorselaars, B.; Michels, M. A. J. *Macromol. Theory Simul.* **2008**, *17*, 290; **2008**, *17*, 393.
(55) Mulder, T.; Harmandaris, V. A.; Lyulin, A.; Van der Vegt, N. F. A.; Kremer, K.; Michels, M. A. J. *Macromolecules*, in press; doi: 10.1021/ma800873z.
(56) Harmandaris, V. A.; Kremer, K., submitted.

(57) Wick, C. D.; Martin, M. G.; Siepmann, J. I. *J. Phys. Chem. B* **2000**, *104*, 8008.
(58) Müller-Plathe, F. M. *Macromolecules* **1996**, *29*, 4782.
(59) Berendsen, H. J. C.; Van der Spoel, D.; Van Drunen, R. *Comput. Phys. Commun.* **1995**, *91*, 43.
(60) Berendsen, H. J. C.; Postma, J. P. M.; Di Nola, A.; Haak, J. R. *J. Chem. Phys.* **1984**, *81*, 3684.
(61) Zoller, P.; Walsh, D. J. *Standard Pressure-Volume-Temperature Data for Polymers*; Technomic: Lancaster, 1995.
(62) Allen, M. P.; Tildesley, D. J. *Computer Simulation of Liquids*; Clarendon: Oxford, 1987.
(63) Hess, B.; Leon, S.; Van der Vegt, N.; Kremer, K. *Soft Matter* **2006**, *2*, 409.
(64) Auhl, R.; Everaers, R.; Grest, G. S.; Kremer, K.; Plimpton, S. J. *J. Chem. Phys.* **2003**, *119*, 12718.
(65) Arnold, A.; Mann, B. A.; Limbach, H. J.; Holm, C. *Comput. Phys. Commun.* **2006**, *174*, 704; see also http://www.espresso.mpg.de/.
(66) Mark, J.; Ngai, K.; Graessley, W.; Mandelkern, L.; Samulski, E.; Koenig, J.; Wignall, G. *Physical Properties of Polymers*, 3rd ed.; Cambridge University Press: Cambridge, 2003.
(67) Fritz, D.; Harmandaris, V. A.; Reith, D.; Van der Vegt, N. F. A.; Kremer, K., in preparation.
(68) Leon, S.; Van der Vegt, N.; Delle Site, L.; Kremer, K. *Macromolecules* **2005**, *38*, 8078.
(69) Wittmer, J.P.l; Beckrich, P.; Johner, A.; Semenov, A. N.; Obukhov, S. P.; Meyer, H.; Baschnagel, J. *Eur. Phys. Lett.* **2007**, *77*, 56003.
(70) Depa, P. K.; Maranas, J. K. *J. Chem. Phys.* **2005**, *123*, 094901.
(71) Depa, P. K.; Maranas, J. K. *J. Chem. Phys.* **2007**, *126*, 054903.
(72) Öttinger, H. *MRS Bull.* **2007**, *32*, 936.
(73) Milner, S. T.; McLeish, T. C. B. *Phys. Rev. Lett.* **1998**, *81*, 725.
(74) Pütz, M.; Kremer, K.; Grest, G. S. *Europhys. Lett.* **2000**, *49*, 735.
(75) Harmandaris, V.; Mavrantzas, V. In *Recent Research Topics and Developments in Chemical Physics: from Nanoscale to Macroscale*; Terzis, A. F., Paspalakis, E., Eds.; Research Signpost: India, 2008.
(76) Evereaers, R.; Sukumaran, S. K.; Grest, G. S.; Svaneborg, C.; Sivasubramanian, A.; Kremer, K. *Science* **2004**, *303*, 823.
(77) Sukumaran, S. K.; Grest, G. S.; Kremer, K.; Evereaers, R. *J. Polym. Sci., Polym. Phys.* **2005**, *43*, 917.
(78) Hoy, R. S.; Robbins, M. O. *Phys. Rev. E* **2005**, *72*, 061802.
(79) Tzoumanekas, C.; Theodorou, D. N. *Macromolecules* **2006**, *39*, 4592.
(80) Tzoumanekas, C.; Theodorou, D. N. *Curr. Opin. Solid State Mater. Sci.* **2006**, *10*, 61.
(81) Larson, R. G. *Macromolecules* **2005**, *38*, 5761.
(82) Kröger, M. *Comput. Phys. Commun.* **2005**, *168*, 209.
(83) Foteinopouloy, K.; Karayiannis, N. C.; Mavrantzas, V. G.; Kröger, M. *Macromolecules* **2006**, *39*, 4207.
(84) Shanbhag, S.; Kröger, M. *Macromolecules* **2007**, *40*, 2897.
(85) Fetters, L. J.; Lohse, D. J.; Richter, D.; Witten, T. A.; Zirkel, A. *Macromolecules* **1994**, *27*, 4639.
(86) Liu, C.; He, J.; van Ruymbeke, E.; Keunings, R.; Baily, C. *Polymer* **2006**, *47*, 4461.
(87) Padding, J.; Briels, W. J. *J. Chem. Phys.* **2004**, *120*, 2996.
(88) Praprotnik, M.; Delle Site, L.; Kremer, K. *J. Chem. Phys.* **2005**, *123*, 224106.
(89) Junghans, C.; Praprotnik, M.; Kremer, K. *Soft Matter* **2008**, *4*, 156.
(90) Delle Site, L.; Abrams, C. F.; Alavi, A.; Kremer, K. *Phys. Rev. Lett.* **2002**, *89*, 156103.
(91) Daoulas, K.; Harmandaris, V.; Mavrantzas, V. *Macromolecules* **2005**, *38*, 5780.
(92) Harmandaris, V.; Daoulas, K.; Mavrantzas, V. *Macromolecules* **2005**, *38*, 5796.
(93) Note that the values of S_{UA-CG} reported here are slightly smaller than the one reported in ref 52 ($S_{UA-CG} = 7.7$). The reason is that all the simulations in this work have been performed at the experimental density, whereas those of ref 52 were executed at *NPT* conditions, which results in a 3−4% higher density.

MA8018624